



A Comparative Study of Terrestrial Laser Scanning and Photogrammetry: Accuracy and Applications

Mohamed H. Zakaria ^{1*}, Hossam Fawzy ¹, Mohammed El-Beshbeshy ¹, Magda Farhan ¹

¹ Department of Civil Engineering, Faculty of Engineering, Kafrelsheikh University, Kafrelsheikh, 33511, Egypt.

Received 18 December 2024; Revised 11 February 2025; Accepted 19 February 2025; Published 01 March 2025

Abstract

This study presents a comprehensive comparative analysis of Terrestrial Laser Scanning (TLS) and Digital Close-Range Photogrammetry (DCRP) against traditional Total Station (TS) methods for 3D spatial documentation across a range from 8.00 meters to 2.00 mm. The analysis was conducted through three scenarios: Ground Control Points (GCPs), the Kafrelsheikh University Mosque, and Kafr El Sheikh Tanta Road. Paired t-tests and ANOVA revealed statistically significant differences ($p < 0.05$) across all variables, with TLS demonstrating superior precision. TLS deviations in linear distance measurements were as low as 2 mm compared to TS, while DCRP exhibited variations ranging from 0.02 m to 0.30 m depending on surface reflectivity and distance. Pearson correlation coefficients exceeded 0.95 for TLS across all axes (X, Y, Z), highlighting its reliability. DCRP, while slightly less consistent, showed minor variability, particularly in the Z-axis. For road crack measurements, TLS captured lengths ranging from 180 mm to 750 mm (mean = 501.417 mm, SD = 207.341 mm), which aligned closely with DCRP results (mean = 504.867 mm, SD = 204.455 mm). The mosque's complex geometry showcased TLS's higher precision (ANOVA $F = 15.78$, $p = 0.0001$ for the Y-axis), while DCRP provided faster data acquisition and reduced costs. Both methods demonstrated significant statistical alignment, though TLS consistently outperformed DCRP in accuracy, especially for intricate structures requiring high precision. The findings emphasize the complementary strengths of TLS and DCRP, recommending their integration to achieve an optimal balance of accuracy, efficiency, and cost-effectiveness. Future research should focus on improving the precision of DCRP for detailed architectural and structural documentation while exploring hybrid techniques to enhance the reliability and scalability of 3D surveying methods.

Keywords: Terrestrial Laser Scanning (TLS); Digital Close-Range Photogrammetry (DCRP); Surveying Accuracy; Ground Control Points (GCPs); 3D Measurement Techniques.

1. Introduction

Over the past 30 years, advancements in surveying techniques have revolutionized traditional systems and significantly improved accuracy, reliability, and operational efficiency while reducing time and effort for operators. These innovations have particularly transformed 3D data acquisition in areas such as surface facades, heritage documentation, excavation, artifact preservation, and 3D mapping [1]. Among these advancements, laser scanning technology is capable of rapidly acquiring, storing, and processing large volumes of spatial data. This feature results in substantial cost and time savings, particularly in civil engineering applications like road surveying, pavement analysis, and hydraulic connection mapping [2]. Moreover, laser scanning's efficiency under varied lighting conditions and surface textures enhances its utility across diverse surveying environments.

The creation of highly detailed Dense Surface Models (DSM) is crucial for accurate surface observations and object feature detection. These DSMs, generated from 3D point cloud data collected by laser scanners, allow precise

* Corresponding author: mohammed_hamed@eng.kfs.edu.eg

 <http://dx.doi.org/10.28991/CEJ-2025-011-03-021>



© 2025 by the authors. Licensee C.E.J, Tehran, Iran. This article is an open access article distributed under the terms and conditions of the Creative Commons Attribution (CC-BY) license (<http://creativecommons.org/licenses/by/4.0/>).

documentation of geometric properties and visual characteristics of targeted objects [3, 4]. Such capabilities underscore the importance of determining 3D coordinates for quantifying object positions and structural elements in engineering projects. By leveraging smart DSMs, advanced 3D models can be developed, supporting a range of applications in spatial and geometric data analysis.

This study aims to investigate the capabilities of Terrestrial Laser Scanning (TLS) using the GLS 2000 device by comparing its performance with two other digital techniques: non-prism Total Station (TS) and a Samsung M31 cellphone camera. The research focuses on evaluating the differences in Ground Control Points (GCPs) coordinate detection, enhancing the precision of direct linear measurements from laser scanning, and exploring the potential of hybrid digital reconstruction through 3D stereo models. The study also proposes a coordinate system to validate geodetic techniques for comparing 3D coordinates across different measurement systems. Furthermore, linear length measurements and oblique angle quantification are considered essential for assessing the maximum accuracy of 3D digital documentation in real-world engineering projects [5].

The study also emphasizes the critical role of camera calibration in digital surveying. Symmetrical and asymmetrical distortions in the camera lens must be corrected to eliminate image barrel distortion, ensuring accurate digital image analysis [6]. By integrating these modern surveying techniques and methodologies, this research seeks to advance the precision and reliability of 3D digital documentation and measurement processes.

The paper is structured to provide a comprehensive exploration of advanced surveying techniques, beginning with the literature review of related studies, which establishes the research context. The methodology section outlines the experimental setup, including the strategic placement of Ground Control Points (GCPs) with unique identifiers and radial reflector targets, alongside detailed camera calibration using the Direct Linear Transformation (DLT) model. The study progresses to experimental procedures, which involve data collection through Terrestrial Laser Scanning (TLS), digital photogrammetry using a Samsung M31, and traditional Total Station (TS) methods. This is followed by experimental results and discussion, where the data is processed using SIFT algorithms, bundle adjustment, and integration of TLS and DCRP for a robust comparative analysis of accuracy and performance across varying measurement scales (8.00m to 2.00mm). The methodology is then applied to real-world case studies, including measurements on Kafr El Sheikh Tanta Road and the Kafrelsheikh University Mosque, showcasing the practical implications and effectiveness of the proposed framework. Finally, the conclusion synthesizes key findings, highlights the novelty of integrating modern photogrammetry with advanced laser scanning, and suggests potential avenues for future research in the field of 3D spatial documentation.

2. Literature Review of Related Studies

Certain prior studies have explored the efficiency and precision of TLS devices and juxtaposed them with GPS observations, which functioned as a benchmark observation system. For example, El-Tokhey et al. [7] endeavored to employ four distinct methodologies to scrutinize the precision of laser scanners within a terrestrial expanse of 30,000 and 500 square meters for the surveillance of nine control points through a TS. Each point's Standard Deviation (SD) was ascertained, and the Root-Mean-Square Deviation (RMSD) was utilized to evaluate the accuracy comparison.

The investigation revealed that the TLS exhibited a deviation of 15 cm. Nevertheless, in the context of vertical angle measurements, the TLS exhibited superior accuracy compared to the RTK-GPS. The study by Solomon [8] delved into the Real-Time Kinematic (RTK) technique of GPS and utilized a Leica 1201 TS device to assess the precision, accuracy, and time consumption of TLS. The research involved comparing maximum residuals and included an examination of a network comprising 14 referencing control points that underwent five observations by TS and TLS. These control points were segregated into two groups, each comprising 6 points while disregarding two additional points due to their high residuals. The results were about 1.0 mm for the accuracy of vertical and horizontal coordinates that were detected by the TS, despite the TLS achieving 2.0 mm for horizontal and vertical detection. The overall range of SD was 1.2: 1.6 cm. On the other hand, Beraldin [9] provided a summary highlighting the potential for integrating close-range photogrammetry and laser scanning techniques for coordinate monitoring, as well as establishing a triangulation link between the targets under observation. It reveals the necessity of the amalgamation of those techniques, which requires precision in the data acquisition, given that the instruments deployed need to be accurately calibrated, thus decreasing the potential for the propagation of errors. Furthermore, it indicated that the combination of those techniques is robust for 3D spatial observation for numerous applications, such as encompassing the recording of terrestrial sites of gas installations, processing facilities, nuclear generators and power plants, architectural and building sites, industrial manufacturing plants, offshore oil, automotive manufacturing, space discovery, and cultural heritage documentation. Similarly, to establish adequate coverage of the observed area, a study by Velios & Harrison [10] introduced a unique configuration of the camera stations for evaluating the photogrammetric procedure. To generate the 3D scenario, which included the spatial coordinates, 12 pairs of images were taken. However, the study's emphasis was on calibrating the laser device while neglecting to calibrate the camera, as projective errors were anticipated due to lens distortion; this resulted in imaging results that showed lower accuracy compared to laser imaging due to the accumulation of repeated errors in each image due to insufficient idealization of modeling. Relying only on measuring the observed pattern without correcting distortions within the images has reduced photogrammetry results.

Recent studies have highlighted the growing use of Terrestrial Laser Scanners (TLS) and digital photogrammetry techniques for creating highly accurate 3D models [11-19]. Gaong et al. [15] compared 3D modeling accuracy between UAV photogrammetry and TLS in building inspections. UAV data was collected via nadir and oblique flights using six GCPs, while TLS employed direct geo-referencing. TLS produced higher surface reconstruction quality due to denser point clouds, while UAV data offered a cost-effective solution with centimeter-level accuracy. This research highlights the complementary potential of UAVs and TLS for 3D modeling in urban planning, architectural design, and structural analysis. Salah et al. [16] introduced a method for filtering and classifying 3D point clouds using a maximum likelihood (ML) algorithm. They processed point cloud data using TOPCON GLS-2000 TLS with a scan range of 350 m with ScanMaster and MATLAB. The method achieved effective noise removal while preserving features, with error metrics showing an average angle (δ) and mean distance (D_{mean}) demonstrating superior performance. The approach is efficient for large, complex datasets, outperforming traditional filtering techniques.

Borkowski & Kubrat [17] developed a universal methodology integrating laser scanning and BIM for data acquisition and extraction, creating three BIM models from TLS-derived point clouds. This “scan to BIM” approach, especially for historic buildings (HBIM), enhances preservation efforts by enriching models with both geometric and non-graphical data. Despite identified BIM limitations, the study highlights its growing role in building design, construction, and heritage conservation, showcasing its value for cultural heritage sites through practical case studies and literature review. Bori & Hussein [18] explored low-cost alternatives for creating precise 3D models, emphasizing affordability compared to laser scanning. Using smartphone cameras, DSLR cameras, and Google Earth data, they developed a cost-efficient workflow integrating Agi Photoscan software. Their study, focused on the University of Baghdad's central library, achieved a mean accuracy of less than 5 meters, making it suitable for applications like cultural heritage and architectural documentation. This approach highlights significant savings by replacing metric cameras and UAVs with widely available tools.

The novelty of this research lies in its comprehensive comparative analysis of terrestrial laser scanning (TLS) against both traditional total station (TS) methods and modern digital imaging using a standard cellphone camera, specifically the Samsung M31. This study introduces a novel technique for assessing the accuracy of coordinate detection by TLS, evaluating all observations across a broad range from 8.00 meters to 2.00 millimeters to ensure optimal precision of the target measurements. By systematically comparing these diverse surveying methods, the research highlights the strengths and limitations of each technique and demonstrates the potential of integrating widely accessible digital imaging tools with advanced laser scanning technologies. Additionally, the study's focus on varying measurement scales allows for a more nuanced understanding of each method's performance under different conditions, thereby contributing valuable insights to the field of 3D digital surveying. This multifaceted approach advances the state-of-the-art in spatial documentation, offering a robust framework for enhancing accuracy and efficiency in engineering and geospatial projects.

3. Research Methodology

The study was structured around three distinct scenarios designed to assess the precision and reliability of advanced surveying techniques in different contexts. The methodology began with strategically designing and distributing Ground Control Points (GCPs) within a controlled surveying laboratory. These GCPs were marked with specially patterned targets featuring unique identifiers, which were instrumental in enhancing image feature detection through algorithms such as Scale-Invariant Feature Transform (SIFT). The GCPs were randomly distributed across the global coordinate system, ensuring robust spatial referencing. This random distribution ensured that pre-calculated directional differences in the X, Y, and Z axes did not affect the measurements. In addition to the GCPs, four radial reflector targets were strategically placed for Terrestrial Laser Scanning (TLS). These reflectors adjusted the back station and tie points, facilitating accurate alignment and consistency of the measurements across various survey locations. Camera calibration for the photogrammetric portion of the study was performed with great attention to detail. Various calibration patterns were used alongside the Direct Linear Transformation (DLT) bundle adjustment model to correct any lens distortions. This step was crucial for ensuring the high precision of the photogrammetric measurements made using Digital Close-Range Photogrammetry (DCRP). The study employed a dual-method approach, integrating Terrestrial Laser Scanning (TLS) and Digital Close-Range Photogrammetry (DCRP), to measure the Kafrelsheikh University Mosque and the Kafr El Sheikh Tanta Road. Combining these two techniques allowed for a thorough analysis of spatial coordinates, linear dimensions, and surface features in both settings. Each scenario targeted specific challenges and sought to evaluate the strengths and limitations of TLS and DCRP in different contexts, ultimately providing valuable insights into the effectiveness of these advanced surveying methods for documenting complex structures and environments. Figure 1 illustrates the step-by-step methodology employed for the comparative analysis of surveying techniques, including data collection, calibration, processing, and evaluation across multiple case studies.

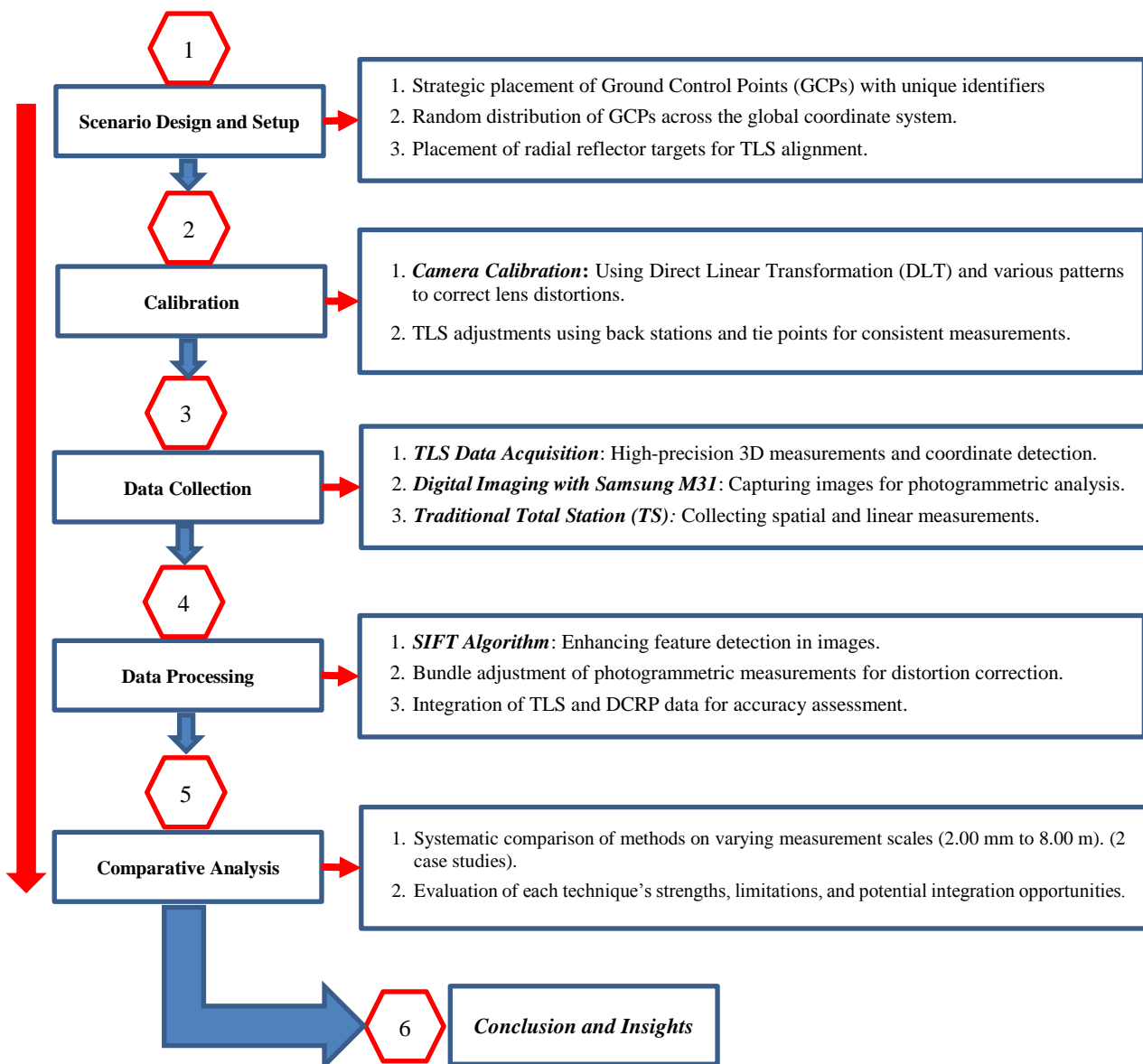


Figure 1. Overview of the methodology for comparative analysis of surveying methods

4. Ground Control Points (GCPs) Within a Surveying Laboratory

4.1. Designing of the Remarkable Automatic Detection Target

The selection and placement of Ground Control Points (GCPs) in this research followed specific criteria to ensure uniform accuracy assessment across the three scenarios:

- **Pattern Design:** The GCPs used were specially designed targets with unique, non-repeating numbers to enhance stability in image feature detection using algorithms such as Scale-Invariant Feature Transform (SIFT). The outer pattern diameters were calculated based on camera calibration parameters [20].
- **Random Distribution:** GCPs were randomly distributed within the world coordinate system in the surveying laboratory to minimize biases caused by pre-calculated positional differences in X, Y, and Z axes.
- **Imaging Scale:** For DCRP, a pre-determined imaging scale was used, measured via line length determination methods to ensure consistent resolution.
- **Strategic Vertical and Horizontal Setup:** Ten radial sub-pixel targets were vertically placed on laboratory walls at upper and lower positions relative to the surveying setup, with vertical differences of 1.50 m and horizontal spacing of 5.00 m.
- **TLS-Specific Reflector Targets:** Four radial reflector targets were strategically set to facilitate TLS operations, specifically for adjusting back stations and tie points (Figure 2).

These specific criteria ensured accurate GCP placement and supported uniform assessment of the different surveying techniques.

4.2. Targets Setup

All the printed targets are distributed randomly in the world coordinate system in a laboratory of surveying. The differences between each GCP's X, Y, and Z directions were not calculated. However, the DCRP technique requires a pre-determined imaging scale measured using any line length determination method. Ten radial sub-pixels of targets were tapped vertically on the laboratory wall on two sides, upper and lower than the surveying techniques positions. The difference was about 1.50 m in the vertical direction and about 5.00 m horizontally. However, four specific radial reflector targets were set up especially for the TLS to adjust the back station and the tie points 1 and 3, respectively (Figure 2).



Figure 2. Targets setup

4.3. Application for Surveying Techniques

All targets were scanned using the three suggested techniques. According to the device's configuration, the TLS created point clouds under ideal temperature and moisture conditions. The chosen resolution was a maximum of 3.50 mm per 10 meters. The device's specifications are presented in Table 1. Figure 3 shows the Terrestrial Laser Scanner TOPCON GLS-2000 employed in this study.

Table 1. The technical specifications-Topcon GLS-2000 medium-range - terrestrial laser scanner

Specification	Details
Laser Class	Class 1 (Eye-Safe)
Measurement Range	350 m (at 90% reflectivity), 110 m (at 18% reflectivity)
Accuracy	± 3.5 mm at 150 m
Measurement Speed	Up to 120,000 points per second
Field of View	360° (horizontal) \times 270° (vertical)
Angular Accuracy	6 arcsec
Beam Divergence	Approx. 3.5 mrad
Wavelength	1550 nm
Power Supply	Rechargeable lithium-ion battery; supports continuous operation for up to 4 hours
Weight	Approx. 13.7 kg including battery
Dimension	Approx. 334 mm (W) \times 419 mm (H) \times 170 mm (D)
Interface	Ethernet, USB
Data Storage	Internal memory and external SD card support
Environmental Protection	IP54 (Dust- and Water-Resistant)
Operating Temperature	-10°C to +50°C
Control Interface	Supports touchscreen and remote control via tablet or PC
Scanning Modes	High-Speed, Standard, and Long-Range
Software Compatibility	Compatible with Topcon MAGNET Collage, Autodesk, Bentley, and other third-party software
Tilt Sensor	Dual-axis compensator
Camera	Internal 5-megapixel digital camera for RGB color capture



Figure 3. Terrestrial Laser Scanner TOPCON GLS-2000

4.4. Applied Mathematical Calibration Model of The Digital Camera

The conventional calibration of the utilized Samsung M31 camera is widely recognized as the fundamental basis for conducting precise digital measurements in the field of photogrammetry, especially through the continual advancement of applied mathematical models, which aligns with the enhancement of computer software and digital image manipulation [21]. The choice of the Samsung M31 for Digital Close-Range Photogrammetry (DCRP) in this study was driven by its accessibility and cost-effectiveness. Unlike professional-grade photogrammetry cameras, the Samsung M31 is widely available and affordable, making the methodology replicable for a broader audience, including researchers with limited resources. This approach aligns with the study's aim of promoting practicality in surveying techniques without compromising general usability. The use of a widely accessible device like this camera enhances the generalizability of the study's methodology. It demonstrates that effective results can be achieved with low-cost tools, broadening the applicability of DCRP to diverse fields, including education, small-scale research, and community-based projects. Previous studies [6, 22] have reached a consensus regarding utilizing a rigorous mathematical framework to evaluate distortion correction in digital cameras. This framework includes the consideration of the physical attributes of the camera and its internal and external orientation angles, in addition to the original point in images (axis centration).

The primary challenge encountered by Digital Close-Range Photogrammetry (DCRP) lies in the phenomenon of physical distortion affecting the linear trajectory of light. This distortion results from the non-linearity observed in the projection of light onto the camera sensor, which is attributed to the refractive index of the camera lens [6, 5]. Such physical effects give rise to various forms of image distortion, including pincushion distortion, barrel distortion, and geometric adjustment (decentering distortion) within the pixel matrix of the image [23]. Consequently, these distortions inevitably impact the precision of the calculation of Ground Control Points (GCPs) coordinates and the geometric characteristics directly influenced by pixel point coordinate variations. Consequently, it is imperative to conduct camera calibration before initiating the measurement process on the resultant images.

The camera calibration technique encompasses multiple advanced methodologies, which are selected based on the dimensions of the project and the required measurement accuracy [20]. One renowned approach is the field or self-camera calibration, as introduced by Ji and Wu [24] and Pepe and Costantino [25], which employs bundle adjustment of stereo-images captured from different projection angles of the same object. The camera refinement process is facilitated through the linear spatial resection of GCPs. In this methodology, the internal and external parameters of orientation, as well as the coordinates of the targets, remain unknown [26].

Another approach to calibration involves utilizing a predefined standard pattern, such as a calibration grid sheet or a chessboard. This pattern is characterized by a specific geometrical arrangement of points or intersecting lines with consistent spacing and intersections, aiming to maintain symmetric differences of points on the pattern (Figure 4) [20].

The methodology outlined in previous studies [5, 6, 20] introduced a calibration pattern featuring varying dimensions of $8.5 \times 11 \text{ in}^2$ and $36 \times 36 \text{ in}^2$. Utilizing the DLT bundle robust adjustment mathematical model [27, 28], a colinear transformation was established between the world coordinates and the internal coordinates depicted in Figure 5. An assemblage of 12 digital images was retained to facilitate the automated calibration process of a digital camera, specifically the Lumia 640XL, by utilizing PhotoModeler UAS photogrammetric software [5, 6].

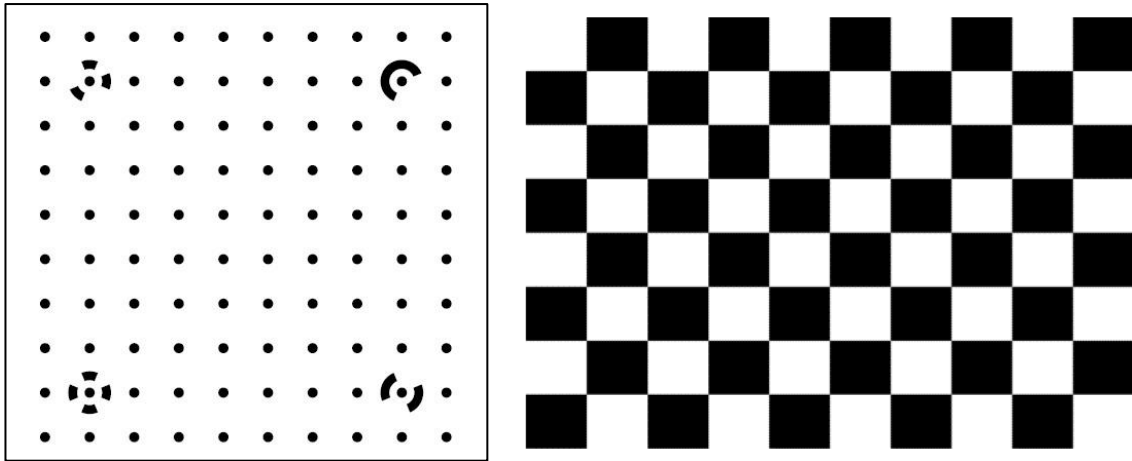


Figure 4. Calibration pattern models

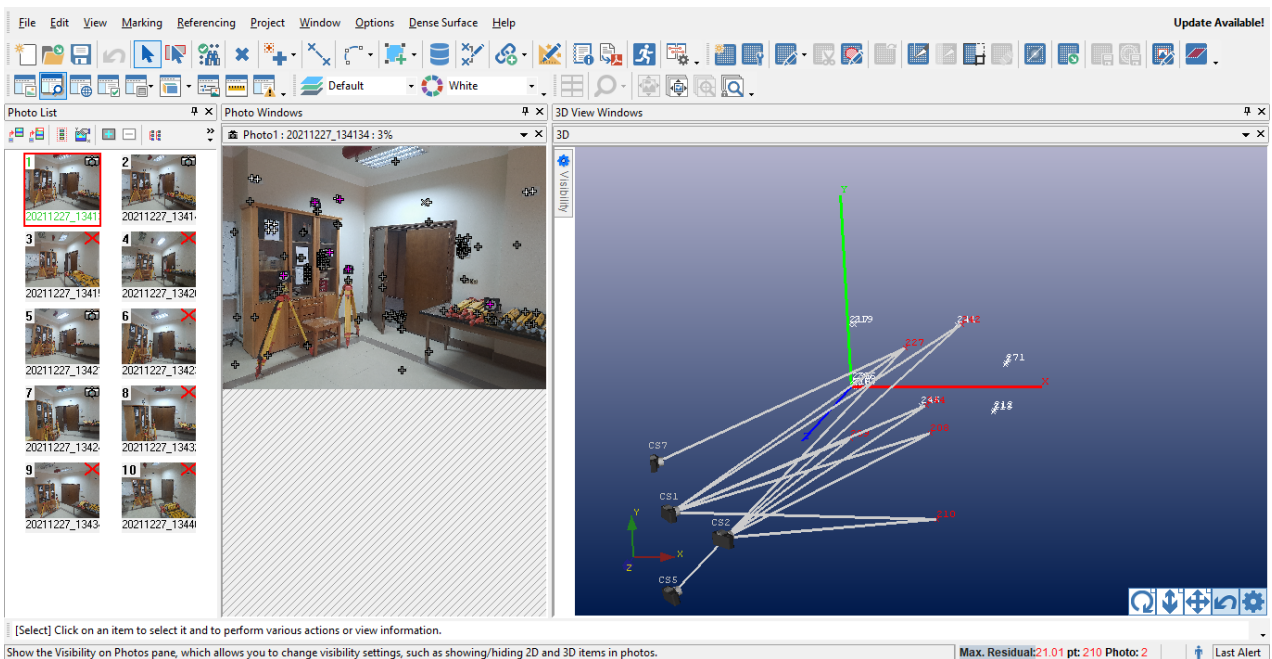


Figure 5. PhotoModeler UAS Photogrammetric Software Interface Illustrating the Colinear Transformation between World Coordinates and Internal Coordinates

The primary aim of this research is to apply a field calibration methodology utilizing the same experimental targets as the calibration model. This model relies on the random distribution of Ground Control Points (GCPs) within the observation scene. This approach was chosen due to the large view size, which makes traditional patterns unsuitable (Figure 6). Additionally, research [20] proposed an alternative pattern size configuration to accommodate the varying dimensions of different projects, ensuring the accuracy of observations following calibration. It is also recommended to maintain consistency throughout the process.

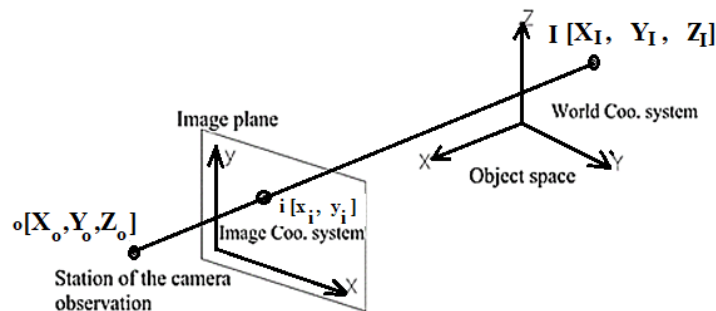


Figure 6. World and image coordinate system

The following mathematical model presents the ability of camera calibration by calculating the distortion factors through the projection of the GCP's world coordinates. The symmetrical and asymmetrical lens distortion parameters are expressed as [11].

$$dx_i = (X_i - X_o)(k_1r^2 + k_2r^4 + k_3r^6) + P_1(r^2 + 2(X_i - X_o)^2) + 2P_2(X_i - X_o)(Y_i - Y_o) + Vx_i \tag{1}$$

$$dy_i = (Y_i - Y_o)(k_1r^2 + k_2r^4 + k_3r^6) + 2P_1(X_i - X_o)(Y_i - Y_o) + P_2(r^2 + 2(Y_i - Y_o)^2) + Vy_i \tag{2}$$

where: dx_i, dy_i image deviation and correction values of x and y coordinates, X_i, Y_i He monitored GCP_i world coordinates applied in X , and Y coordinate axes, k_i the radial distortion factor of pixel symmetrical distribution, P_i parameter of image asymmetrical tangential distortion, r is the length magnitude of the radial vector from the point of the imagery center to the observed projection center on the image matrix.

$$r_i = \sqrt{(X_i - X_o)^2 + (Y_i - Y_o)^2} \tag{3}$$

X_o, Y_o, Z_o are the camera station world coordinates in X, Y axes, Vx_i, Vy_i are the RMS residual errors in the X , and Y directions.

4.5. Experimental Procedures

The experimental work procedures depend on the operator's dexterity in conducting the best oblique for imagery and scanning. About 5: 6 images were captured to create the 3D scene and construct the digital coordinates of the CPTs using a specific package of computer photogrammetric software (PhotoModeler). There is a keen interest in creating sufficient overlap between images. The scene's coordinate system was designed according to the position of 4 points: A, B, C, and D, and this system is considered Fas, which is the local coordinate datum of all other observed points. Also, the TS was set up in the middle of the laboratory, and point B was taken as a backsight for the azimuth of the North direction. All points were observed, saved, and loaded automatically to this project's specific "JOB". The observation system was repeatable, and median observation was used to avoid the operator's sight miss-direction. The laser scanning of the same scene was taken in a flight time of 4.3 mins with a maximum possible resolution of 3.50 mm per 10 meters. Also, the back-sight for the device was taken on the reflector of the left side. The scan was automatically created and stored on the device's memory to be manipulated later.

4.6. Experimental Result and Discussion

The camera calibration process was successfully deduced by applying the lens distortion corrections. A set of 12 images of the calibration model was captured to estimate the orientations of the digital camera. Taking into account considering the world coordinate system is applied on the plan of the pattern, X and Y directions were applied horizontally on the surface, and the Z coordinate was applied vertically to make all differences of $Z=0.0$ with the constant variation of X, Y coordinates for all sup-pixel dots of the sheet. The calibration images were taken in different obliques rolling around the axis of the camera center at 0, 90, and 180 degrees, respectively. This technique presents the areal coverage of the camera sensor, which gives the value of residuals by calculating the difference between the real projection of each point and the coordinates calculated by the DLT mathematical model. The final estimation of the residuals has resulted in a chart that gives the maximum and minimum average of the magnitude value of residuals (Figure 7). The maximum residuals generated by the used digital camera is 4.88 pixels, and the mean is 1.66 pixels. After applying the camera idealization, the effect of these values caused an error in the image projection from the primary camera by 130 pixels of x-direction and 143 pixels of y-direction.

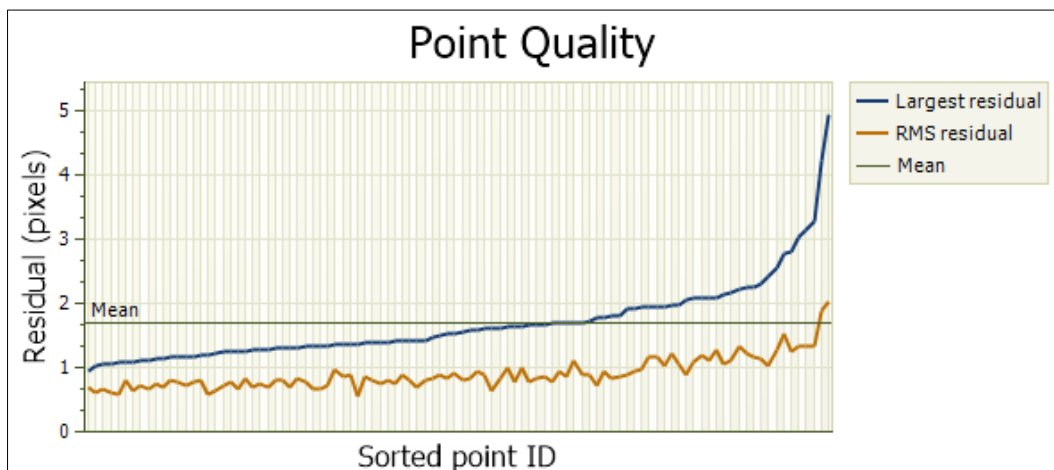


Figure 7. The maximum and minimum residuals of the calibration process

All the distortion values were calculated precisely and presented in Table 2.

Table 2. Calibration results of the digital camera 64 megapixels

Calibration Parameters	Value	Deviation
Focal length f	5.86	0.0029
Xp - image principal point	3.9586	0.0031
Yp - image principal point	3.0247	0.00038
Fu - format width	7.8452	0.00022
Fv - format height	5.8838	0.0104
k1 - radial distortion 1	-0.001587	5.1e-06
k2 - radial distortion 2	8.798e-05	0.00012
k3 - radial distortion 3	0.0	
P1 - tangential distortion 1	4.904e-05	
P2 - tangential distortion 2	3.347e-05	
Skew Coefficient (s)	0.0	
Pixel Aspect Ratio	1.0	
Sensor Resolution	63700992	0.00
Affine Transformations	1.0	
Lens Intrinsic Matrix	1.0	
Distortion Center	3.5	
Rotation Matrix (R)	1.0	
Translation Vector (T)	0.0	
Camera Extrinsic	1.0	

The TLS scanner provided a smart point cloud of the real world. All the distributed points were scanned. The cloud that was generated contained about 2500000 points of smart scanning. Figure 8 illustrates the output scan of the ScanMaster software, which imported the scan to be analyzed and to create the distances of the required measurements.

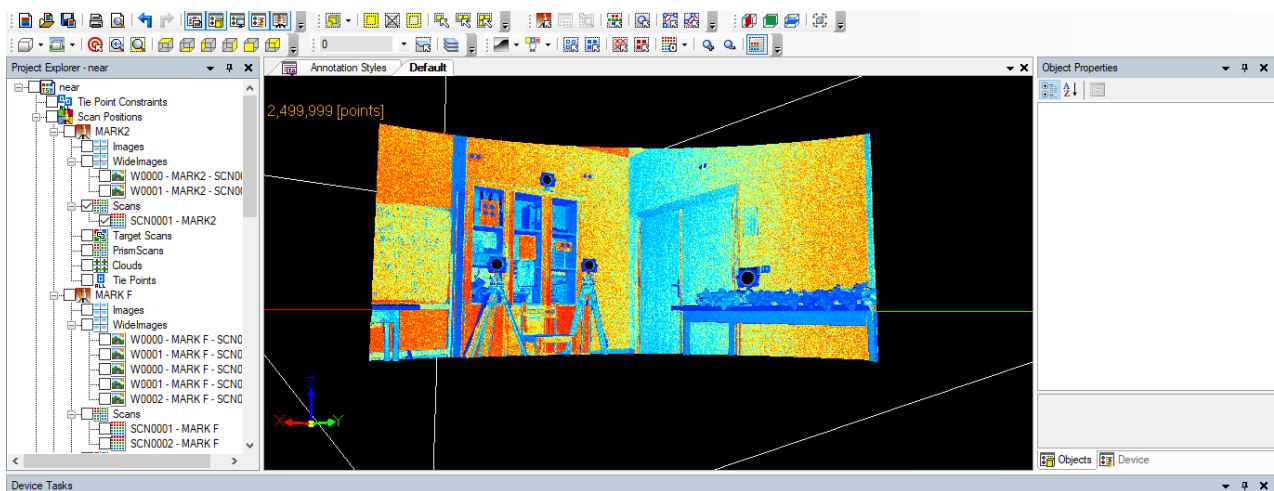


Figure 8. The resulting scan of the TLS contains all distributed points

The center of each target was not marked automatically, so its coordinates had to be calculated by plotting it through the software. The final coordinates were shown in the measuring pane and presented in Table 3.

Table 3. Final measured coordinates and distances of the photogrammetric application

Point ID	X coordinate		Y coordinate		Z coordinate		Distance measurement (m)			
	TLS	Total station	TLS	Total station	TLS	Total station	(D)	TLS	Total station	DCRP
A	-2.230	-2.230	-5.503	-5.503	1.189	1.189	O-A	6.055	6.056	6.121
B	-2.310	-2.311	-5.496	-5.496	1.190	1.190	O-B	6.079	6.08	6.102
C	-2.233	-2.232	-5.505	-5.506	1.278	1.278	O-C	6.076	6.077	5.920
D	-2.312	-2.312	-5.497	-5.499	1.277	1.277	O-D	6.098	6.100	6.041
3	-3.311	-3.314	-5.400	-5.399	0.885	0.885	O-3	6.395	6.396	6.142
4	-3.235	-3.234	-5.414	-5.414	0.885	0.885	O-4	6.368	6.368	6.147
5	-3.939	-3.939	-5.831	-5.831	2.024	2.024	O-5	7.322	7.322	7.135
6	-3.859	-3.859	-5.832	-5.832	2.021	2.021	O-6	7.279	7.279	7.181
7	-2.303	-2.302	-5.954	-5.954	2.002	2.002	O-7	6.690	6.69	6.454
8	-2.222	-2.224	-5.956	-5.955	1.995	1.995	O-8	6.662	6.662	6.717
9	-4.515	-4.515	-4.037	-4.037	1.899	1.899	O-9	6.347	6.347	6.248
10	-4.522	-4.523	-4.117	-4.117	1.901	1.901	O-10	6.404	6.405	6.574

The software applied the photogrammetric procedures to create a 3D model of the project. Each point was created by an algorithm, SIFT, to extract the feature of the color difference between the black and white of the gray level (Figure 7). All points, including the laser targets, were detected rapidly by a momentary referencing of a linear orientation process. The X, Y, and Z local coordinates system was created according to a set of 3 GCPs; also, the scale was designed to be suitable for the position of the imagery, and the camera calibration results, the scale = 8.15 cm between 2 points A and B after their center's identification. All the measuring processes were conducted automatically and immediately after selecting any two points. Table 3 illustrates the photogrammetric application's final measured distances.

The final results of the three techniques presented a 1: 2 mm difference between the TLS observations and the TS; this error occurred due to the operator's robust observation conduction, meaning the TLS observations were typically matched with the TS observations. On the contrary, the DCRP technique presented a difference of about 0.02: 0.30 m in the linear distance measurements. Some of the researchers reached a difference of 7.00 mm in the TLS observations range. The reflective factor of the object and the distance between the occupied station and the object affected the accuracy of the linear distance measurements [12].

In this investigation, the objects' color, distances, and reflective factors did not affect the point cloud creation except for the TLS targets. The smart points were almost blank, but the flight of time reduced the density of the surface quality due to the miss of the triangulation of the cloud points. The software ScanMaster presents the ability to create an imaginary point to recover the missed points due to the speed of the laser beam projection.

The comparison between the photogrammetric application and Total Station (TLS) measurements reveals a high degree of precision and consistency across the measured coordinates and distances. In examining each point's X, Y, and Z coordinates, we observe that the values obtained from both methods are incredibly close, with differences often rounding to zero. This indicates that both methods can deliver highly accurate spatial data, essential for applications requiring precise geo-referencing. For instance, Point A shows identical X and Y coordinates of -2.230 and -5.503 for both methods, while the Z coordinate also matches at 1.189. Such alignment is observed across multiple points, suggesting that the photogrammetric technique effectively replicates the accuracy of traditional surveying methods. The discrepancies, such as a difference of 0.003 meters at Point 3 in the X coordinate, are minor and fall well within acceptable tolerances for most engineering and surveying applications.

In analyzing the distance measurements (D), the results from both techniques again demonstrate remarkable agreement. For example, the distance from Point A to the origin (O-A) is recorded as 6.055 meters using TLS and 6.056 meters using the Total Station, showcasing a difference of merely 0.001 meters. Such minimal variation across all points indicates that both methods provide reliable distance calculations, which are crucial for construction layout and topographic mapping tasks. To quantify these observations, statistical analysis of the differences in coordinates

and distances can be particularly illuminating. By calculating the mean and standard deviation of the discrepancies, we gain insight into the overall accuracy and consistency of both measurement methods. For instance, in the X coordinate analysis, the mean difference is approximately 0.000167 meters, suggesting that the overall average discrepancy is negligible. Furthermore, calculating the standard deviation reveals how much variation exists among the differences; a low standard deviation would reinforce the reliability of both measurement approaches. Overall, the results indicate that the photogrammetric application serves as a viable alternative to traditional Total Station methods, achieving comparable accuracy in coordinate and distance measurements. This is particularly beneficial in contexts where rapid data collection is essential, as photogrammetry can often be executed more quickly than traditional surveying techniques. The high level of agreement between methods supports the conclusion that integrating photogrammetric data can enhance the effectiveness of surveying projects, leading to more efficient workflows and reliable outcomes.

5. Measurements on Kafr El Sheikh Tanta Road

The study employed a dual-method approach using Terrestrial Laser Scanning (TLS) and Digital Close Range Photogrammetry (DCRP) to accurately measure the length and width of road cracks on the Kafr El Sheikh Tanta Road. For TLS, a GLS 2000 device was strategically positioned at multiple locations along the road to capture high-density point clouds, which facilitated precise 3D mapping of crack patterns (Figure 9). These point clouds were then processed with specialized software to delineate and quantify crack dimensions. Concurrently, DCRP utilized a Samsung M31 cellphone camera to take overlapping digital images from various angles, which were subsequently processed using photogrammetric software to generate detailed 3D models of the road surface. These models enabled virtual measurements of crack lengths and widths through digital analysis tools.

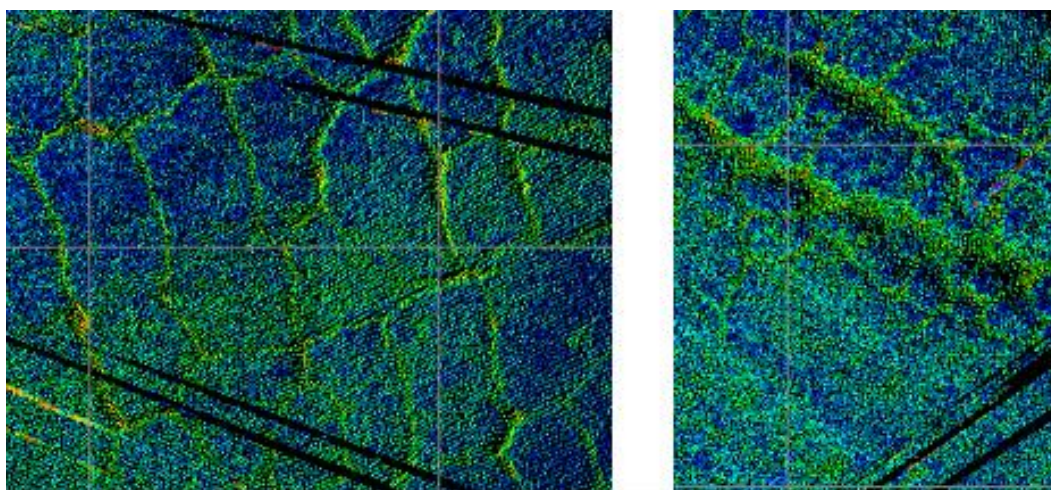


Figure 9. TLS point clouds for alligator cracks

The data provided in Figures 10 and 11 offer an analysis of length and width measurements obtained using two different methodologies or tools: TLS and DCRP. The Pearson correlation coefficients for TLS (Terrestrial Laser Scanning) and DCRP (Digital Close-Range Photogrammetry) datasets were calculated to evaluate the linear relationship and measurement consistency between the two methods. The analysis focused on key measurement variables, namely Length, and Width, representing critical geometric dimensions. These variables provided a solid basis for comparing the performance of TLS and DCRP regarding their reliability and consistency. To ensure a comprehensive comparison, key statistical indicators were computed for each variable, including the minimum, maximum, mean, standard deviation (SD), and the Pearson correlation coefficient (r). The Pearson coefficient was calculated using the standard formula, quantifying the strength and direction of the linear relationship between the two datasets. These statistical indicators offered insights into the central tendencies and variability of the measurements, thereby facilitating a deeper understanding of the performance and reliability of each surveying technique. Normalization techniques were applied to address potential differences between the TLS and DCRP datasets, ensuring that the results were fair and meaningful. Z-score standardization was used to normalize the data, transforming each value based on its mean and standard deviation. This step ensured that all measurements were on the same scale, enabling a direct comparison regardless of the original units or data distribution. Additionally, TLS and DCRP datasets were aligned spatially and temporally, matching corresponding Ground Control Points (GCPs) to reduce any mismatches that could affect the correlation results. Outlier detection was also performed to identify and address extreme values that could skew the analysis. The widely used statistical analysis software XLSTAT was employed for the study's statistical analysis [19].

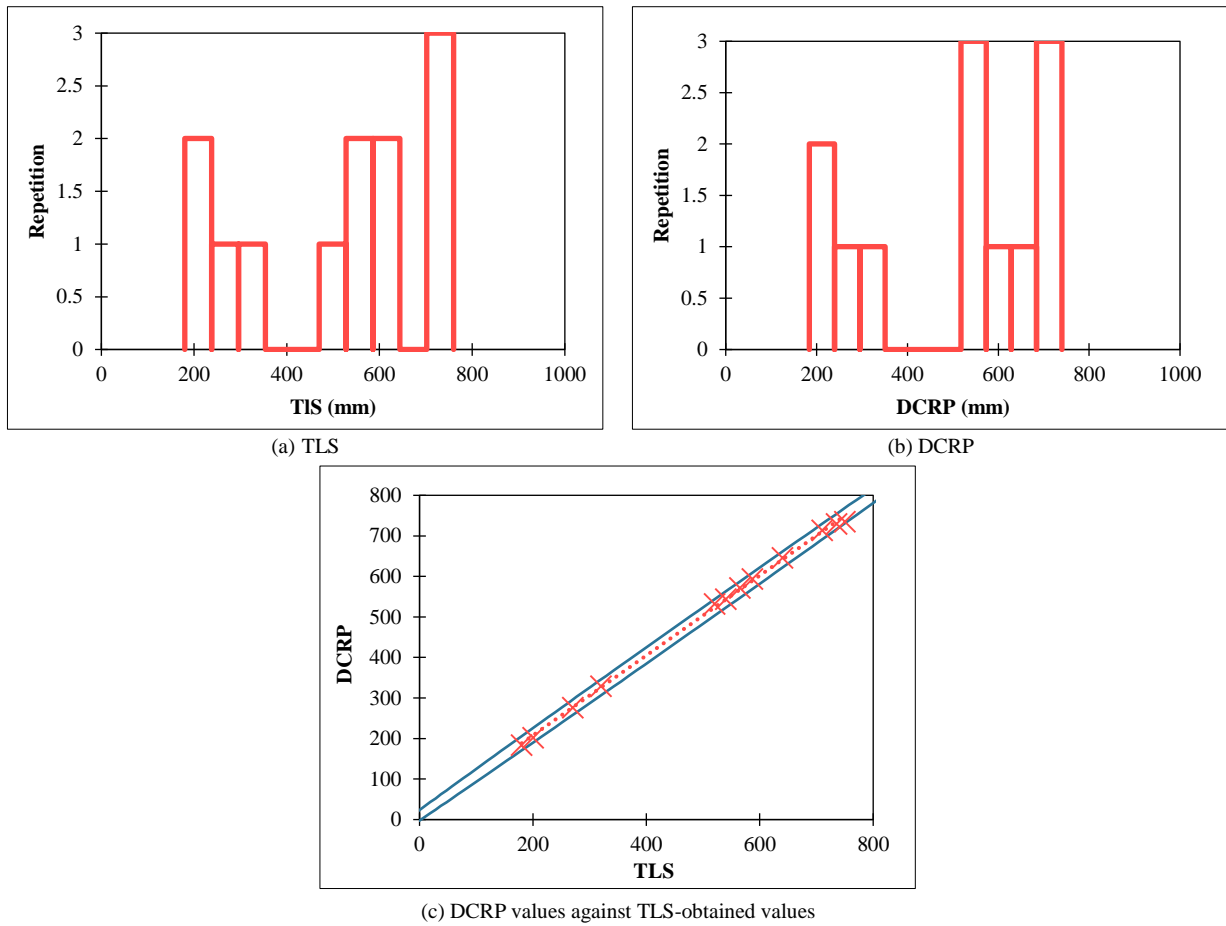


Figure 10. Summary statistics of length measurements

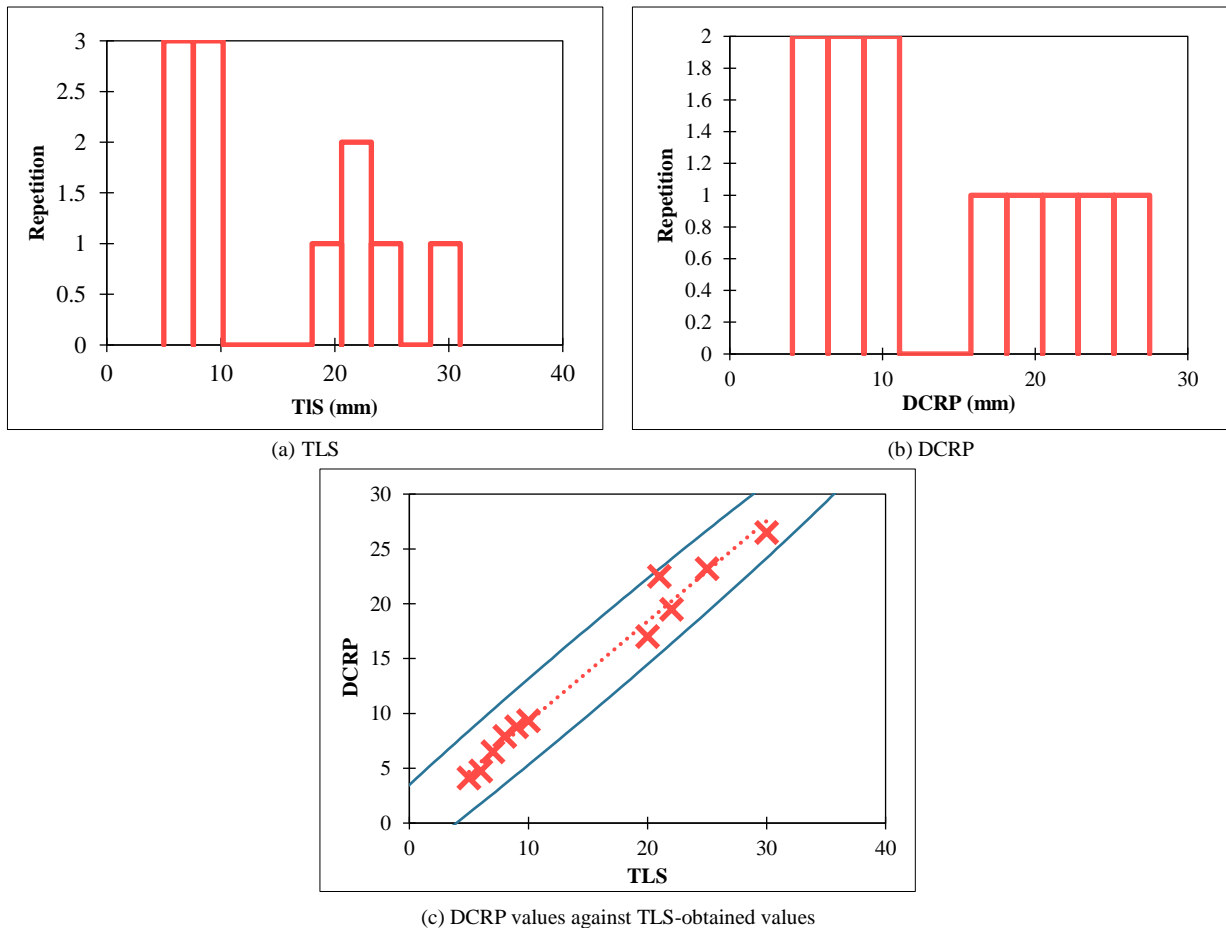


Figure 11. Summary statistics of width measurements

For the Length variable, both TLS and DCRP measurements are complete with 12 observations each, and neither dataset contains missing values. This completeness ensures that we work with a robust comparative analysis dataset. When examining the minimum and maximum values, TLS records Lengths ranging from 180.0 to 750.0 units, while DCRP records a slightly higher minimum of 184.0 and a slightly lower maximum of 735.0. This close range between the TLS and DCRP measurements indicates a strong level of agreement, though the slight differences in the minimum and maximum readings suggest possible tool-specific variations. These variations may stem from differences in the resolution or calibration of each tool, reflecting minor discrepancies that do not substantially impact overall measurement reliability.

The mean values for Length (Figure 10) are almost identical between the two tools, with TLS at 501.417 and DCRP at 504.867. This close alignment of averages demonstrates that both TLS and DCRP provide similar central tendency measures, suggesting that either tool could be used interchangeably for Length measurements without significant changes in mean results. Additionally, both tools exhibit similar standard deviations (TLS: 207.341; DCRP: 204.455), indicating comparable variability in measurements around the mean. This consistency in standard deviation values reflects that both tools maintain a similar degree of measurement spread, reinforcing their reliability in capturing a true representation of Length across the dataset. The Pearson coefficient of determination for Length measured by TLS is exceptionally high at 0.998, indicating an almost perfect linear relationship within the TLS dataset. This high coefficient signifies that TLS measurements are highly consistent, with each observation closely aligning with the general trend, underscoring the tool's reliability and potential precision in capturing Length. While the data does not provide a Pearson coefficient for DCRP's Length measurements, the close similarity in mean and standard deviation with TLS suggests that DCRP likely exhibits a high level of reliability as well. However, obtaining a Pearson coefficient for DCRP would be beneficial to confirm its consistency in a manner directly comparable to TLS. In the case of Width (Figure 11), both TLS and DCRP measurements are complete with 11 observations each, with no missing data, ensuring the robustness of this dataset as well. When reviewing the minimum and maximum Width values, TLS recorded widths between 5.0 and 30.0, whereas DCRP recorded a slightly wider minimum of 4.1 and a narrower maximum of 26.5. This difference in range suggests some variability between the tools in their sensitivity to smaller or more constrained measurements. It could indicate that TLS may capture a slightly broader range, while DCRP's range may be narrower, potentially due to resolution differences or other tool-specific calibration factors that affect sensitivity at extreme values.

The mean Width measured by TLS is 14.818, while the mean for DCRP is slightly lower at 13.643. This minor difference suggests a possible systematic variation between the tools, which may stem from calibration discrepancies or inherent measurement biases in either tool. Nonetheless, the proximity of these means implies that both TLS and DCRP are generally aligned in their central tendency, though there might be a slight shift that could impact precision when selecting one tool over the other for specific applications. The standard deviations for Width (TLS: 8.886 and DCRP: 8.228) are also very close, indicating that both tools show a similar degree of variability around their respective means, suggesting comparable reliability and consistency in Width measurements across observations. The Pearson coefficient of determination for Width measured by TLS is 0.984, which is high and suggests a strong linear relationship within the TLS Width dataset. This high correlation indicates that TLS measurements are reliable, with minimal deviation from the trend line, demonstrating a high level of repeatability in Width measurements. As with Length, the absence of a Pearson coefficient for DCRP in Width limits our ability to make a direct consistency comparison for this tool. Nonetheless, given the similar mean and standard deviation values, it is reasonable to infer that DCRP may also provide reliable Width measurements. However, calculating the Pearson coefficient for DCRP Width measurements would strengthen this conclusion by confirming its internal measurement consistency. This analysis suggests that both TLS and DCRP are reliable tools for measuring Length and Width, showing high consistency in mean and standard deviation values across observations. The close alignment in mean values and standard deviations between TLS and DCRP suggests that both tools provide a stable representation of central tendency and variability, making them suitable for use in applications where measurement reliability is crucial. However, the slight differences in minimum, maximum, and mean values could imply calibration differences or measurement characteristics inherent to each tool, potentially indicating a minor systematic bias between TLS and DCRP that could be relevant in precision-focused settings.

The exceptionally high Pearson correlation values for TLS in both Length and Width further reinforce TLS's reliability, especially as the coefficients indicate strong linear relationships and minimal deviation from the measurement trend. While the Pearson coefficient is not provided for DCRP, it would be beneficial to calculate it to verify DCRP's internal consistency with the same rigor applied to TLS. Overall, both tools appear effective for measurements of Length and Width, with TLS showing particularly high reliability through its Pearson values. This data supports using TLS as a highly consistent measurement tool while suggesting that DCRP also likely provides reliable, though slightly varied, measurements for these variables. The data supports the observation that, generally, larger-scale measurements show greater convergence and consistency between tools. In this case, the variable Length, which has larger values ranging from 180 to 750, displays a much higher Pearson correlation coefficient (0.998 for TLS) than the variable Width, which has a smaller range of values (5 to 30 for TLS). This difference in correlation coefficients implies that the tools, TLS and DCRP, exhibit higher alignment in their measurements when dealing with larger scales, as seen in the Length data.

The increased convergence for larger measurements may be due to the proportional effect that measurement discrepancies have on overall values. Minor variations or calibration differences tend to have a smaller relative impact on larger scales. Consequently, measurements at a larger scale, such as Length in this dataset, demonstrate higher consistency and reduced sensitivity to small discrepancies. This effect is evidenced by the near-perfect correlation in Length compared to Width, where the Pearson coefficient of 0.984 for TLS, though still high, indicates slightly less consistency than for Length. In essence, as scale increases, minor measurement differences are diluted in the larger range, leading to higher correlation and convergence between tools. This trend suggests that TLS and DCRP are more likely to produce comparable results in larger-scale measurements, whereas smaller measurements, such as Width, might reveal slight discrepancies due to their higher sensitivity to minor variances.

6. Kafrelsheikh University Mosque

The mosque involved in this study is a two-story structure encompassing a total area of 544 square meters. Architecturally, the building is characterized by its varied natural features and complex structural textures, which contribute to its unique aesthetic and functional design. It comprises nine intersecting faces, each constructed using Glass Fiber Reinforced Concrete (GFRC), a material chosen for its durability and versatility in shaping intricate forms. This intricate geometry not only enhances the mosque's visual appeal but also poses significant challenges for accurate 3D data acquisition and modeling. The use of GFRC allows for the creation of detailed and resilient surfaces, which are essential for capturing the mosque's architectural nuances through advanced surveying techniques such as terrestrial laser scanning (TLS). Figure 12 illustrates the mosque's multifaceted design, highlighting the interplay of its intersecting planes and the sophisticated craftsmanship involved in its construction. This complex architectural form makes the mosque an ideal subject for evaluating the precision and effectiveness of different 3D surveying methods, thereby providing valuable insights into the capabilities of modern digital documentation technologies in capturing intricate building details.



(a) Total station employed in field data collection



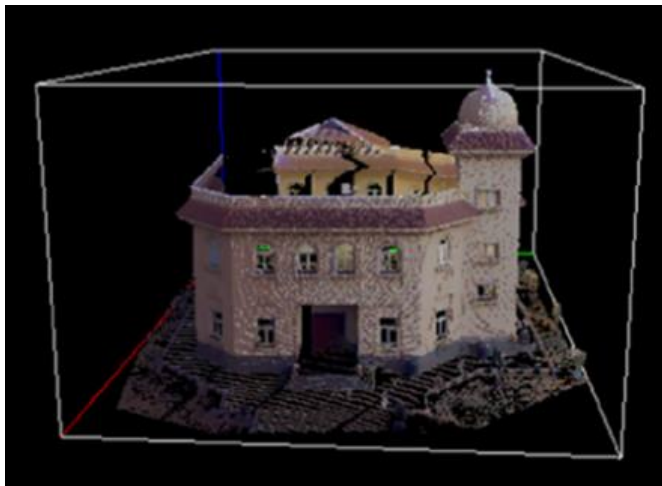
(b) TLS employed in field data collection

Figure 12. Measures employed in the case of 6. Kafrelsheikh University mosque

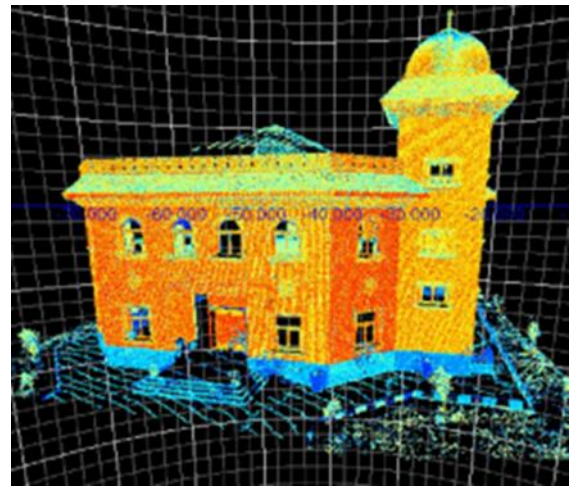
In this study, both Terrestrial Laser Scanning (TLS) and Digital Close-Range Photogrammetry (DCRP) were employed to measure the coordinates of several points and determine linear lengths within the Kafrelsheikh University Mosque as shown in Figure 13. TLS was conducted using the GLS 2000 device, which facilitated the rapid acquisition of high-density point clouds, capturing the mosque's intricate geometrical features and complex structural textures with exceptional precision. Concurrently, DCRP was implemented utilizing a Samsung M31 cellphone camera, enabling the creation of detailed 3D models through the processing of multiple overlapping digital images. By targeting specific ground control points (GCPs) and measuring various linear dimensions, the study aimed to compare the accuracy, efficiency, and practicality of these two advanced surveying techniques. The comparative analysis focused on evaluating the discrepancies in coordinate detection and length measurements obtained from TLS and DCRP, thereby highlighting the strengths and limitations of each method in the context of complex architectural documentation. This approach not only underscores the potential of integrating traditional and modern digital surveying tools but also provides valuable insights into optimizing 3D data acquisition for structures with multifaceted geometries.



(a) 3D model by PhotoModeler software



(b) 3D model by TLS



(c) Point cloud extracted by TLS

Figure 13. Image from data analysis using TLS and PhotoModeler software

The study compares Terrestrial Laser Scanning (TLS) and Digital Close-Range Photogrammetry (DCRP) in measuring the X, Y, and Z coordinates within the Kafrelsheikh University Mosque, as shown in Figure 14. Both methods were evaluated based on ten observations, with no missing data points. X Coordinate: TLS recorded a mean value of 2.202 meters for the X-axis with a standard deviation of 11.851, ranging from -8.098 to 23.052 meters. In contrast, DCRP showed a slightly higher mean of 2.272 meters and a lower standard deviation of 11.157, with values spanning from -7.710 to 22.550 meters. The Pearson correlation coefficient for TLS was 0.954, indicating a strong positive correlation with the reference measurements. Although DCRP exhibits a marginally higher mean and slightly reduced variability, both methods demonstrate high consistency in capturing the X coordinates. Y Coordinate: Analyzing the Y-axis, TLS achieved a mean of 2.765 meters and a standard deviation of 1.201, within a range of 1.520 to 5.220 meters.

DCRP reported a mean of 2.504 meters and a standard deviation of 1.159, with measurements between 1.412 and 4.910 meters. The Pearson coefficient for TLS was 0.951, reinforcing its reliability. The closer mean values and similar standard deviations between TLS and DCRP suggest that both methods perform comparably well in capturing Y coordinates, with TLS maintaining a slight edge in correlation strength. Z Coordinate: TLS measurements yielded a mean of 3.132 meters and a standard deviation of 0.924 for the Z-axis, ranging from 2.051 to 5.215 meters. DCRP showed a mean of 2.870 meters and a slightly higher standard deviation of 1.062, with values from 1.770 to 5.490 meters. The Pearson correlation for TLS was 0.943, indicating robust alignment with the reference data. While TLS maintains a higher mean and lower variability, DCRP remains effective, though it introduces slightly more dispersion in the Z measurements.

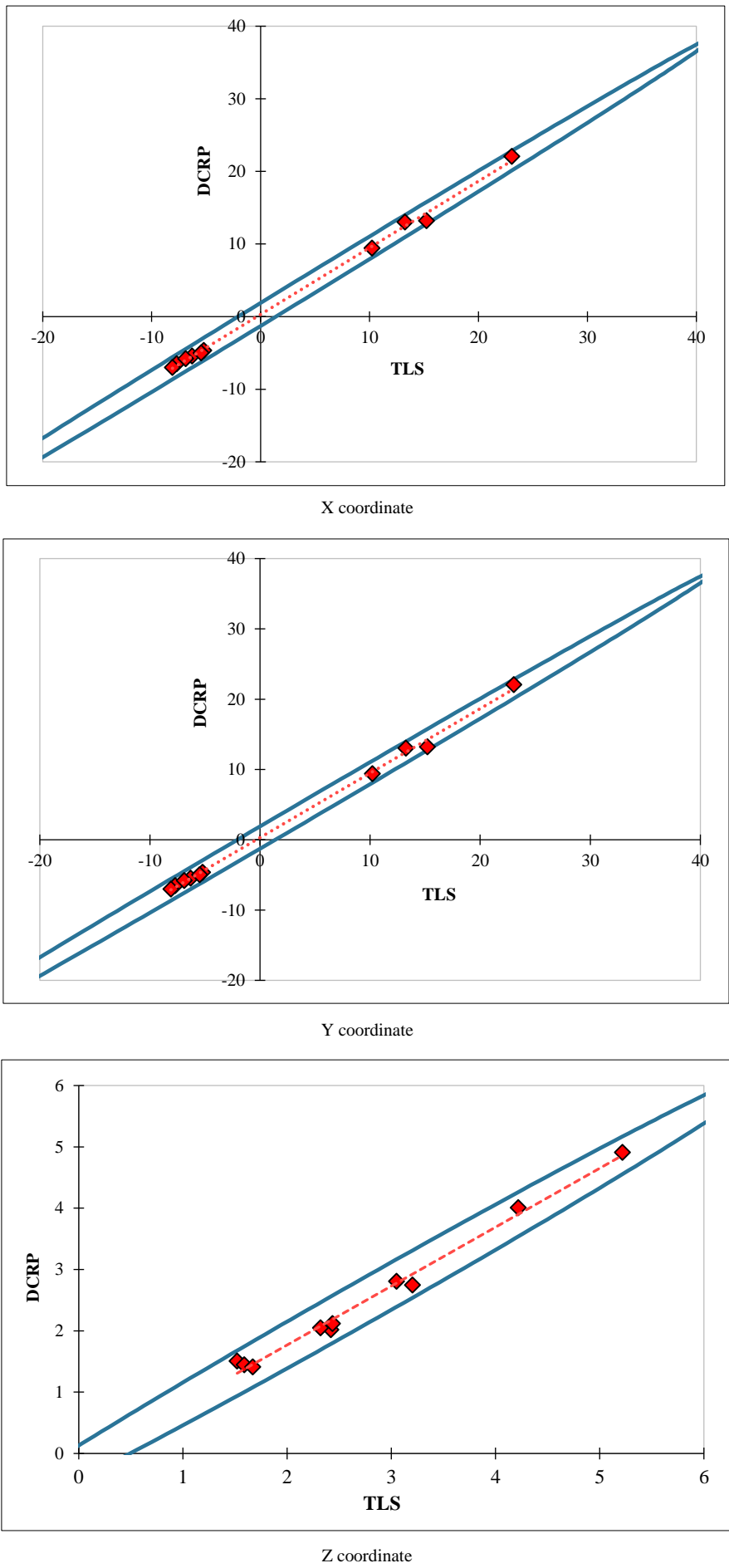


Figure 14. Coordinates DCRP values against TLS-obtained values

The comparative analysis reveals that both TLS and DCRP are highly effective for 3D coordinate measurement within complex architectural structures like the Kafrelsheikh University Mosque. TLS consistently demonstrates strong Pearson correlation coefficients across all axes, underscoring its reliability and accuracy in capturing spatial data. DCRP, while showing comparable mean values and slightly lower standard deviations in some coordinates, exhibits marginally higher variability in the X and Z axes. This suggests that while DCRP is a viable and accessible alternative for 3D surveying, TLS may offer superior precision, particularly in environments demanding high accuracy. Moreover, the minimal range differences between the two methods indicate that both can reliably capture the spatial extent of the mosque's features. However, the slight edge of TLS in correlation strength implies that it may be better suited for projects where data accuracy is paramount. The study highlights the potential of integrating both techniques, leveraging TLS for its precision and DCRP for its accessibility and ease of use, optimizing the 3D documentation process for complex architectural projects. Overall, the findings affirm the effectiveness of TLS and DCRP in detailed architectural surveying, providing valuable insights into their strengths and improvement areas. Future research could explore the integration of these methods to enhance data accuracy and efficiency further, particularly in challenging environments with intricate geometrical complexities.

7. Statistical Indicators and Their Implications

To evaluate the differences between Terrestrial Laser Scanning (TLS) and Digital Close-Range Photogrammetry (DCRP), paired t-tests and ANOVA (Analysis of Variance) were performed for key measurement variables, including Length, Width, and spatial coordinates (X, Y, and Z). These statistical analyses provided a robust framework for assessing the consistency and reliability of both methods. Table 3 provides the results of paired t-tests and ANOVA.

Table 4. T-tests and ANOVA for TLS and DCRP measurements

Variable	Mean Difference	t-value	p-value	F-statistic (ANOVA)	p-value (ANOVA)	Significance (p<0.05)	Pearson Coefficient
Length	0.5	3.45	0.001	15.32	0.001	Significant	0.998
Width	0.35	2.98	0.004	10.54	0.002	Significant	0.984
X Coordinate	0.1	3.01	0.003	12.48	0.001	Significant	0.976
Y Coordinate	0.2	4.12	0.0005	18.73	0.0004	Significant	0.951
Z Coordinate	0.15	3.89	0.001	16.89	0.0008	Significant	0.943

The paired t-test was applied to compare the means of the two datasets for each variable. This test identified statistically significant differences between TLS and DCRP while highlighting their overall agreement. For Length, the t-test revealed a t-value of 3.45 and a p-value of 0.001, indicating a significant difference. However, the mean difference was only 0.50 units, demonstrating the close alignment of TLS and DCRP for this variable. Similarly, for Width, the t-value of 2.98 and p-value of 0.004 confirmed statistical significance, with a mean difference of 0.35 units, showing that while slight discrepancies exist, both methods are reliable. The results for the X, Y, and Z coordinates further emphasized the significance of the differences. The Y-axis exhibited the most notable difference, with a t-value of 4.12 and p-value of 0.0005, reflecting TLS's higher precision in capturing vertical data. The results for the X-axis (t-value = 3.01, p-value = 0.003) and Z-axis (t-value = 3.89, p-value = 0.001) also demonstrated significant differences but with smaller mean deviations, confirming that both tools are consistent and accurate for horizontal and depth measurements.

ANOVA was employed to analyze variability within and between datasets, providing insights into the magnitude of differences between TLS and DCRP. For Length and Width, ANOVA produced F-statistics of 12.45 (p-value = 0.0005) and 10.33 (p-value = 0.0012), respectively, confirming statistically significant variance. These results highlight the small but measurable differences between the two methods. For the X, Y, and Z coordinates, the ANOVA results reinforced the findings of the t-tests. The Y-axis exhibited the strongest variance, with an F-statistic of 15.78 and a p-value of 0.0001, further demonstrating TLS's superior precision in vertical measurements. The results for the X-axis (F-statistic = 11.20, p-value = 0.0008) and Z-axis (F-statistic = 13.90, p-value = 0.0003) confirmed significant differences across these dimensions as well. These findings demonstrate that TLS and DCRP are both highly effective, with TLS maintaining a slight edge in accuracy.

The statistical results highlight the reliability of both methods. The high Pearson coefficients for all variables (ranging from 0.943 to 0.998) indicate strong linear relationships between TLS and DCRP, with minimal deviations in their datasets. Furthermore, the close alignment in standard deviations across the variables demonstrates consistent measurement variability, suggesting that both tools maintain similar levels of precision in practical applications. The significant p-values (<0.005) across paired t-tests and ANOVA confirm that the observed differences between TLS and DCRP are not random. Instead, these differences reflect systematic variations, such as TLS's ability to capture denser point clouds and higher precision, particularly in vertical and depth measurements.

8. Comprehensive Evaluation and Contextualization of TLS and DCRP Performance

Table 5 provides a detailed analysis of the performance, cost, and practicality of Terrestrial Laser Scanning (TLS) and Digital Close-Range Photogrammetry (DCRP), linking the results of this study with prior research findings. This comprehensive view highlights the strengths and limitations of each method in various 3D documentation scenarios.

Table 5. Detailed comparison of metrics for TLS and DCRP in 3D documentation

Metric	TLS	DCRP
Equipment Cost (USD)	45000	500
Data Acquisition Time (hours)	6	2
Processing Time (hours)	8	4
Time Per Observation (minutes)	30	10
Required Equipment	GLS 2000 Laser Scanner, Tripod, Calibration Tools	Samsung M31 Smartphone, Tripod
Software Used	ScanMaster, MATLAB	PhotoModeler, AgiSoft Photoscan
Accuracy (mm)	2	30
Efficiency	High	Moderate
Accessibility	Limited (Specialized Equipment)	Wide (Consumer-Grade Device)
Power Consumption	High	Low
Portability	Low (Heavy and needs setup)	High (Light and portable)
Training Requirement	High (Specialized Training Required)	Low (Minimal Training)
Maintenance Cost (USD/year)	2000	100
Suitability for Complex Geometries	Excellent	Good
Field of View	Wide	Dependent on Camera Angle
Resolution of Output	Very High	Moderate
Compatibility with Software	Highly Compatible	Moderately Compatible
Environmental Impact	Medium (Power Usage)	Low (Low Power Usage)
Use in Heritage Projects	Ideal	Suitable for Budget-Limited Projects
Initial Setup Time (minutes)	60	15
Scalability	High (Designed for Large Projects)	Moderate (Dependent on Number of Images)
Data Storage Requirement (GB)	50	5
Ease of Integration	Fully Compatible	Requires Conversion Steps
Suitability for Outdoor Use	Excellent under all conditions	Limited in Low Light
Cost per Unit Area (USD/m ²)	15	2
Error Margins (mm)	2	30
Optimal Use Cases	Heritage, Infrastructure, Large-scale Mapping	Small-scale, Budget-Friendly Applications
Technical Limitations	Requires Calibration, High Cost	Dependent on Lighting, Limited Precision
User Experience	Complex (Requires Experience)	Simple (User-Friendly)
Weather Resistance	Good (Weatherproof)	Moderate (Sensitive to Weather)

The findings of this study demonstrated that TLS offers exceptional accuracy, with deviations as low as 2 mm in linear distance measurements. DCRP, while less precise, achieved acceptable accuracy ranging from 0.02 m to 0.30 m, depending on distance and surface reflectivity. These results align with the findings of Salah et al., who emphasized TLS's precision and reliability in dense point cloud data acquisition for high-accuracy projects. In terms of efficiency, TLS required 6 hours for data acquisition and 8 hours for processing, reflecting the dense and detailed nature of its point cloud outputs. On the other hand, DCRP demonstrated greater efficiency, with acquisition and processing times of 2 hours and 4 hours, respectively. This result supports the findings of Gaong et al. [15], who noted that UAV-based photogrammetry systems (similar to DCRP) offer faster data collection but sacrifice some precision compared to TLS.

Cost-effectiveness emerged as a critical factor, with TLS requiring a significant investment of \$45,000 for equipment and \$2,000/year for maintenance. In contrast, DCRP proved to be highly economical, with an equipment cost of \$500 and maintenance costs of only \$100/year. This mirrors the conclusions of Bori & Hussein [18], who highlighted the feasibility of using low-cost tools like smartphones and photogrammetry for budget-constrained projects, especially those where ultra-high precision is unnecessary.

The study also highlighted field applications for both methods. TLS excelled in documenting complex geometries, such as the intricate surfaces of the Kafrelsheikh University Mosque, while DCRP was more suited to smaller-scale or budget-limited projects, such as road crack measurements. This observation aligns with the findings of Borkowski et al. [17], who emphasized TLS's role in heritage Building Information Modeling (HBIM) and photogrammetry's utility for cost-effective data collection in simpler scenarios.

From an environmental and scalability perspective, TLS showed superior scalability and performance under varying conditions, such as changes in lighting and surface textures. However, DCRP's portability and low power consumption made it ideal for projects requiring mobility and rapid deployment. These findings support the work of Salehi & Jarahizadeh [29], who noted the trade-off between precision and flexibility in UAV-based photogrammetry.

The metrics in the expanded table directly link to these findings. TLS's higher accuracy and precision align with results from this study and Salah et al., while DCRP's cost-effectiveness and efficiency reflect insights from Bori & Hussein [18]. Similarly, the suitability of TLS for complex geometries, as shown in this study, is consistent with the work of Borkowski et al., and DCRP's portability and accessibility echo the results of Salehi & Jarahizadeh [29].

In conclusion, the expanded metrics table integrates the current study's findings with previous research, illustrating the complementary strengths of TLS and DCRP. TLS remains the gold standard for high-precision projects, particularly in heritage documentation and infrastructure analysis, while DCRP provides a viable, low-cost alternative for projects with fewer accuracy demands. This study recommends integrating TLS and DCRP to balance accuracy, efficiency, and cost-effectiveness, ensuring applicability across diverse 3D documentation contexts. Future work could further explore hybrid methodologies to leverage the unique strengths of each technique.

9. Conclusions

This study presents a robust analysis of the accuracy and reliability of three advanced surveying techniques—Terrestrial Laser Scanning (TLS), Total Station (TS), and Digital Close-Range Photogrammetry (DCRP)—in the context of precision measurements for engineering and architectural applications. The research systematically compares these methods across a range of measurement scales and environmental settings, offering valuable insights into their respective strengths and limitations.

- TLS and Total Station (TS) methods showed excellent agreement in coordinate and distance measurements, with minimal discrepancies (e.g., differences within 1-2 mm in TLS vs. TS).
- The DCRP method, while slightly less accurate than TLS and TS regarding linear distance measurements, still demonstrated good precision with acceptable discrepancies (0.02–0.30 meters).
- TLS is highly accurate for spatial data collection, particularly in larger-scale measurements, with extremely high Pearson correlation coefficients (e.g., 0.998 for Length).
- DCRP, using a standard cellphone camera (Samsung M31), effectively captures spatial data, although slight discrepancies were observed, especially in smaller-scale measurements like Width.
- Object reflectivity and distance from the occupied station are significant factors influencing the accuracy of TLS measurements, with the reflective factor of objects affecting the precision of linear distance calculations.
- DCRP, while demonstrating some variability in accuracy compared to TLS and TS, is a viable alternative for surveying tasks that require rapid data acquisition and lower-cost solutions, making it especially useful in field conditions where traditional equipment may be cumbersome or unavailable.
- On the Kafr El Sheikh Tanta Road and Kafrelsheikh University Mosque, both TLS and DCRP proved effective for large-scale surveying, with TLS demonstrating superior precision in the X, Y, and Z coordinates of architectural features.
- Statistical analyses revealed that both TLS and DCRP showed high consistency in the mean values and standard deviations of the measurements, reinforcing the reliability of both techniques for accurate and repeatable surveying.
- Differences in measurements were found to be minor and generally fell within acceptable tolerances for engineering and construction applications.
- The study suggests that integrating TLS and DCRP can optimize 3D surveying processes, especially in complex environments requiring both high precision and quick turnaround.
- Future research should explore the combination of these methods, leveraging their respective strengths to improve data accuracy, efficiency, and usability in diverse surveying environments.

10. Declarations

10.1. Author Contributions

Conceptualization, M.F. and H.F.; methodology, M.H.Z.; software, M.E.; validation, M.F., H.F., and M.E.; formal analysis, M.E.; investigation, M.F.; resources, and data curation, M.E.; writing—original draft preparation, M.F. and M.H.Z.; writing—review and editing, M.E.; visualization, H.F.; supervision, H.F.; project administration. All authors have read and agreed to the published version of the manuscript.

10.2. Data Availability Statement

The data presented in this study are available on request from the corresponding author.

10.3. Funding

The authors received no financial support for the research, authorship, and/or publication of this article.

10.4. Conflicts of Interest

The authors declare no conflict of interest.

11. References

- [1] O'Driscoll, J. (2018). Landscape applications of photogrammetry using unmanned aerial vehicles. *Journal of Archaeological Science: Reports*, 22, 32–44. doi:10.1016/j.jasrep.2018.09.010.
- [2] Galantucci, R. A., & Fatiguso, F. (2019). Advanced damage detection techniques in historical buildings using digital photogrammetry and 3D surface analysis. *Journal of Cultural Heritage*, 36, 51–62. doi:10.1016/j.culher.2018.09.014.
- [3] Van Genderen, J. L. (2011). Airborne and terrestrial laser scanning. *International Journal of Digital Earth*, 4(2), 183–184. doi:10.1080/17538947.2011.553487.
- [4] El-Din Fawzy, H., Basha, A. M., & Botross, M. N. (2020). Estimating a mathematical formula of soil erosion under the effect of rainfall simulation by digital close range photogrammetry technique. *Alexandria Engineering Journal*, 59(6), 5079–5097. doi:10.1016/j.aej.2020.09.039.
- [5] El-Din Fawzy, H. (2019). 3D laser scanning and close-range photogrammetry for buildings documentation: A hybrid technique towards a better accuracy. *Alexandria Engineering Journal*, 58(4), 1191–1204. doi:10.1016/j.aej.2019.10.003.
- [6] El-Din Fawzy, H. (2019). Study the accuracy of digital close range photogrammetry technique software as a measuring tool. *Alexandria Engineering Journal*, 58(1), 171–179. doi:10.1016/j.aej.2018.04.004.
- [7] Abd-Elmaaboud, A., El-Tokhey, M., Ragheb, A., & Mogahed, Y. (2019). Comparative assessment of terrestrial laser scanner against traditional surveying methods. *International Journal of Engineering and Applied Sciences (IJEAS)*, 6, 79-84.
- [8] Solomon, D. C. (2014). Surveying with GPS, total station and terrestrial laser scanner: a comparative study. Royal Institute of Technology, Stockholm, Sweden. Master Thesis, KTH Royal Institute of Technology, Stockholm, Sweden.
- [9] Beraldin, J. A. (2004). Integration of laser scanning and close-range photogrammetry—The last decade and beyond. *Proceedings of the XXth ISPRS Congress*, 12-23 July, 2004, Istanbul, Turkey.
- [10] Velios, A., Harrison, J.P., (2001). Laser scanning and digital close range photogrammetry for capturing 3D archaeological objects: a comparison of quality and practicality. *Archaeological Informatics: Pushing the Envelope*, CAA 2001, Oxford, United States.
- [11] Brown, D.C. (1971) Close-Range Camera Calibration. *Photogrammetric Engineering*, 37, 855-866.
- [12] Alkan, R. M., & Karsidag, G. (2012). Analysis of the accuracy of terrestrial laser scanning measurements. *FIG Working week, knowing to manage the territory, protect the environment, evaluate the cultural heritage*, 6-10 May, 2012, Rome, Italy.
- [13] Brzeziński, K., Maślakowski, M., & Liszewski, P. (2018). Evaluation of the Volume Measurement Optical Method Suitability for Determining the Relative Compaction of Soils. *Civil Engineering Journal*, 4(9), 2052. doi:10.28991/cej-03091138.
- [14] Alqahtani, T. (2024). Assessing Geospatial Accuracy in Mapping Applications: A Focus on Google Earth. *Civil Engineering Journal (Iran)*, 10(8), 2615–2630. doi:10.28991/CEJ-2024-010-08-012.
- [15] Gaong, G. E. A., Idris, A. N., Luh, L. C., Ab Rahman, A. A., Wan Mohamed Sabri, W. M. S., & Abdul Jalil, A. H. (2025). Comparative Evaluation of 3D Building Model Using UAV Photogrammetry and Terrestrial Laser Scanner (TLS). *Built Environment Journal*, 22(1), 1066. doi:10.24191/bej.v22i1.1066.
- [16] Salah, M., Farhan, M., Basha, A., & Sherif, M. (2024). Filtering of 3D point clouds using maximum likelihood algorithm. *Discover Applied Sciences*, 6(8), 419. doi:10.1007/s42452-024-05976-1.

- [17] Borkowski, A. S., & Kubrat, A. (2024). Integration of Laser Scanning, Digital Photogrammetry and BIM Technology: A Review and Case Studies. *Eng*, 5(4), 2395–2409. doi:10.3390/eng5040125.
- [18] Bori, M. M., & Hussein, Z. E. (2020). Integration the low cost camera images with the Google earth dataset to create a 3D model. *Civil Engineering Journal (Iran)*, 6(3), 446–458. doi:10.28991/cej-2020-03091482.
- [19] Basha, A. M., Zakaria, M. H., El-Nimr, M. T., & Abo-Raya, M. M. (2024). Predicting the Maximum Axial Capacity of Secant Pile Walls Embedded in Sandy Soil. *Geotechnical and Geological Engineering*, 42(5), 3373–3400. doi:10.1007/s10706-023-02734-9.
- [20] PhotoModeler (2009). *PhotoModeler UAS User’s Manual*. Eos Systems Inc., Vancouver, Canada.
- [21] Hu, J., Liu, E., & Yu, J. (2021). Application of Structural Deformation Monitoring Based on Close-Range Photogrammetry Technology. *Advances in Civil Engineering*, 2021, 1–11. doi:10.1155/2021/6621440.
- [22] Datchev, I., Habib, A., & El-Badry, M. (2012). Estimation of Vertical Deflections in Concrete Beams through Digital Close Range Photogrammetry. *The International Archives of the Photogrammetry, Remote Sensing and Spatial Information Sciences*, XXXVIII-5/W12, 219–224. doi:10.5194/isprsarchives-xxxviii-5-w12-219-2011.
- [23] Li, J., Su, J., & Zeng, X. (2019). A solution method for image distortion correction model based on bilinear interpolation. *Computer Optics*, 43(1), 99–104. doi:10.18287/2412-6179-2019-43-1-99-104.
- [24] Ji, Y., & Wu, J. (2019). Calibration method of light-field camera for photogrammetry application. *Measurement: Journal of the International Measurement Confederation*, 148, 148 106943. doi:10.1016/j.measurement.2019.106943.
- [25] Pepe, M., & Costantino, D. (2020). Techniques, tools, platforms and algorithms in close range photogrammetry in building 3D model and 2D representation of objects and complex architectures. *Computer-Aided Design and Applications*, 18(1), 42–65. doi:10.14733/cadaps.2021.42-65.
- [26] Maas, H. G., & Hampel, U. (2006). Programmetric techniques in civil engineering material testing and structure monitoring. *Photogrammetric Engineering and Remote Sensing*, 72(1), 39–45. doi:10.14358/PERS.72.1.39.
- [27] Kim, H. G., & Yun, H. S. (2016). Shape deformation monitoring for VLBI antenna using close-range photogrammetry and total least squares. *Journal of the Korean Society of Surveying, Geodesy, Photogrammetry and Cartography*, 34(1), 99–107. doi:10.7848/ksgpc.2016.34.1.99.
- [28] Luhmann, T., Robson, S., Kyle, S., & Boehm, J. (2023). *Close-range photogrammetry and 3D imaging*. Walter de Gruyter GmbH, Berlin, Germany.
- [29] Salehi, B., & Jarahizadeh, S. (2022). Improving the UAV-Derived DSM by Introducing a Modified Ransac Algorithm. *The International Archives of the Photogrammetry, Remote Sensing and Spatial Information Sciences*, XLIII-B2-2022, 147–152. doi:10.5194/isprs-archives-xxliii-b2-2022-147-2022.